Supplementary Information

for

Mechanosynthesis of bifunctional FeNi-N-C oxygen electrocatalyst via a facile mixed-phase templating and preheating-pyrolysis.

Akmal Kosimov,[a] Gulnara Yusibova,[a] Ivan Tito Wojsiat,[a] Jaan Aruväli,[b] Maike Käärik,[a] Jaan Leis,[a] Peeter Paaver,[b] Sergei Vlassov,[c] Arvo Kikas,[c] Vambola Kisand,[c] Helle-Mai Piirsoo,[c] Kaupo Kukli,[c] Ivo Heinmaa,[d] Tiit Kaljuvee,[e] Nadezda Kongi*[a]

[a]*Institute of Chemistry, University of Tartu, Ravila 14a, 50411, Tartu, Estonia*
[b]*Institute of Ecology and Earth Sciences, University of Tartu, Ravila 14a, 50411, Tartu, Estonia*
[c]*Institute of Physics, University of Tartu, Ostwaldi 1, 50411, Tartu, Estonia*
[d]*National Institute of Chemical Physics and Biophysics (NICPB), Acadeemia tee 23, 12618, Tallinn, Estonia*
[e]*Department of Materials and Environmental Technology, Tallinn Technical University, Ehitajate tee 5, 19086 Tallinn, Estonia*

* Corresponding author: nadezda.kongi@ut.ee (Nadezda Kongi)

Experimental Section

Materials and methods

2,4,6-tri(2-pyridyl)-1,3,5-triazine (tripyridyl triazine – TPTZ, ≥ 98%, Sigma-Aldrich), 2,4,6-Triamino-1,3,5-triazine (Melamine-99% Alfa Aesar), Iron(III) chloride hexahydrate ($FeCl_3 \cdot 6H_2O$ ≥ 98% Sigma-Aldrich), Nickel(II) chloride hexahydrate ($NiCl_2 \cdot 6H_2O$ ≥ 98% Sigma-Aldrich), hydrochloric acid (HCl ≥ 37%, Honeywell-Fluka), Potassium chloride (KCl 99.0-100.5%, Sigma-Aldrich). The KCl was pulverized in a ball mill to achieve an average crystallite size of 300–800 nm. Nafion perfluorinated resin solution (5 wt%, Sigma-Aldrich). Ultrapure water (18.2 MΩ cm; Milli-Q purification system by Millipore) was used to prepare all solutions. Milling was conducted in a ball mill (Retsch MM400) using 5 mL zirconium oxide milling jars and 5 mm diameter zirconium oxide milling balls. A tubular furnace (Carbolite Gero EST 12/300B) was used for the carbonization.

Synthesis of catalysts

IroNi-3D: To synthesize the templated catalyst 150 mg (0.48 mmol) of 2,4,6-tri(2-pyridyl)-1,3,5-triazine (TPTZ), 196 mg (1.55 mmol) of 2,4,6-Triamino-1,3,5-triazine (melamine), 137.7 mg (0.57 mmol) of NiCl2·$6H_2O$, 310.5 mg (310.5 mmol) of $FeCl_3 \cdot 6H_2O$ and 468.5 mg (6.3 mmol) of KCl were placed in a milling jar with 360 µL of 1 M HCl solution and milled at 25 Hz for 10 minutes. Pyrolysis was performed in 2 uninterrupted steps, firstly the FeNi-TPTZ was preheated at 300 ˚C for 1 hour with a heating rate of 10 °C min^{-1}, then carbonized at 800 ˚C for 1 hour at the same heating rate. Hydrothermal washing was performed at 80 °C for 1 hour, with continuous stirring, and the catalyst was then filtered and dried – the final mass of IroNi-3D – 128 mg.

IroNi-2: To synthesize the non-templated catalyst 150 mg (0.48 mmol) of 2,4,6-tri(2-pyridyl)-1,3,5-triazine (TPTZ), 196 mg (1.55 mmol) of 2,4,6-Triamino-1,3,5-triazine (melamine), 137.7 mg (0.57 mmol) of $NiCl_2 \cdot 6H_2O$ and 310.5 mg (310.5 mmol) of $FeCl_3 \cdot 6H_2O$ were placed in a milling jar with 360 µL of 1 M HCl solution and milled at 25 Hz for 10 minutes. Pyrolysis was performed in 2 uninterrupted steps, firstly the FeNi-TPTZ was preheated at 300 ˚C for 1 hour with a heating rate of 10 °C min^{-1}, then carbonized at 800 ˚C for 1 hour at the same heating rate. Hydrothermal washing was performed at 80 °C for 1 hour, with continuous stirring, and the catalyst was then filtered and dried – the final mass of IroNi-2 – 113 mg.

IroNi-1: To synthesize the non-templated and non-C/N-doped catalyst 150 mg (0.48 mmol) of 2,4,6-tri(2-pyridyl)-1,3,5-triazine (TPTZ), 137.7 mg (0.57 mmol) of $NiCl_2 \cdot 6H_2O$ and 310.5 mg (310.5 mmol) of $FeCl_3 \cdot 6H_2O$ were placed in a milling jar with 360 µL of 1 M HCl solution and milled at 25 Hz for 10 minutes. Pyrolysis was performed in 2 uninterrupted steps, firstly the FeNi-TPTZ was preheated at 300 °C for 1 hour with a heating rate of 10 °C min^{-1}, then carbonized at 800 °C for 1 hour at the same heating rate. Hydrothermal washing was performed at 80 °C for 1 hour, with continuous stirring, and the catalyst was then filtered and dried – the final mass of IroNi-1 – 104 mg.

Physical characterization

Powder X-Ray Diffraction (PXRD)

The PXRD analysis was carried out using Bruker D8 Advance diffractometer with Ni-filtered Cu Kα as a radiation source and LynxEye line detector. The powder samples were measured in a range of 3° to 93° 2θ using a scanning step of 0.013° 2θ and a counting time of 356 s per step.

Thermogravimetric analysis (TGA)

The TG-DTA experiments with a Setaram Labsys Evo 1600 thermoanalyzer were carried out in Ar atmosphere in the following order: at first, the samples were heated up to 300 °C at the heating rate of 10 °C min^{-1} under non-isothermal conditions with following storing samples at this temperature one hour, then, the temperature was increased up to 800 °C at the heating rate of 10 °C min^{-1} under non-isothermal conditions with following storing the samples also at this temperature one hour, after that the samples were cooled down to 30 °C at the heating rate of 50 °C min^{-1} under non-isothermal conditions. Standard 100 µL alumina crucibles were used, the mass of the samples was between 6.0-6.9 mg, and the gas flow was 20 mL min^{-1}.

Solid-state Nuclear Magnetic Resonance (NMR)

Solid state ^{13}C MAS NMR spectra were recorded on Bruker AVANCE-II spectrometer at 14.1 T magnetic field using a probe for 1.8 x 15 mm Si_3N_4 rotors, 39 kHz fast spinning speed, spin-echo pulse sequence ($\pi/2 - \tau - \pi - \tau -$ acquisition) and relaxation delay 200 ms. Each spectrum was averaged by 400000 accumulations. These spectra show mainly the resonances of carbons attached

to the metal ions, where carbons have fast relaxation and large deviation of chemical shifts due to the hyperfine interaction.

In addition, to see only the resonances of aromatic TPTZ carbons attached to the protons, we recorded the spectra with a probe for 4 mm rotors at 12.5 kHz spinning speed with ordinary $^{1}H/^{13}C$ cross-polarization technique followed by high field proton decoupling (CP-MAS NMR) as well. All chemical shifts are given in the TMS scale.

The spectra in Fig. S7 show that despite several changes in the ^{13}C CP-MAS NMR spectra due to loading the metal ions, all the resonances of the aromatic carbons show chemical shifts like that of pristine TPTZ.

Microwave Plasma Atomic Emission Spectroscopy (MP-AES)

MP-AES was used to analyze the concentration of metals in the bulk of the catalyst samples. The analysis was performed with Agilent 4210 MP-AES. Analytical wavelengths were set to Fe 371.993 nm. Microwave digestion (Anton Paar Multiwave PRO system) was utilized for sample preparation to dissolve the catalyst materials (10 mg each) in a mixture of 2 mL of H_2O_2 and 4 mL of HNO_3 in NXF100 vessels (PTFE/TFM liner). Digestion parameters were temperature – 230 °C pressures in the range of 45 and 50 bar. Afterward, dilution to 5 mg L^{-1} of metal concentration was carried out with 2% HNO_3.

Nitrogen physisorption measurements

The porosity parameters of the prepared materials were determined by low-temperature N2 adsorption with a NOVAtouch LX2 (Quantachrome Instruments). Prior to measurement, each sample was degassed in a vacuum at 300 °C for 12 hours. The materials' BET surface area (SBET) was calculated with a P/P0 interval of 0.02 - 0.2. The total pore volume (Vtot) was calculated with a value of P/P0 of 0.97. Density functional theory (DFT) data (specific surface area (S_{dft}), the volume of micropores (V_{μ}), and pore size distributions (*PSD*) were estimated from N_2 isotherms using a quenched solid density functional theory (QSDFT) equilibria model (QSDFT N_2 – carbon equilibrium transition kernel at 77 K based on slit-pore model) in pressure range 0.006-1 using TouchWin ver. 1.22 software. [1]

Scanning Electron Microscopy (SEM)

SEM images were acquired on FEI Nova NanoSEM 450 at 3 kV.

X-ray Photoelectron Spectroscopy (XPS)

XPS was conducted at ultra-high vacuum conditions using a non-monochromatic twin anode X-ray tube (Thermo XR3E2) with the characteristic energy of 1,253.6 eV (Mg K_α) and an electron energy analyzer SCIENTA SES 100. Samples were prepared by deposition of suspension of the catalytic materials in isopropanol at a concentration of 4 mg mL^{-1} onto GC plates (1.1×1.1 cm). The survey scan was collected using the energy range from 900 to 0 eV, pass energy of 200 eV, step size of 0.5 eV, step duration of 0.2 s, and a scans number of 5. High-resolution XPS scans were performed using pass energy 200 eV and step size 0.1 eV. An Ag wire attached to the sample holders was used for energy reference (Ag 3d5/2 at 367.8 eV); no charging effects were observed. Peak fitting was done using CasaXPS (version 2.3.16) software. The Gauss–Lorentz hybrid function (GL 70, Gauss 30%, Lorentz 70%) and a blend of linear and Shirley-type backgrounds were used for peak fitting.

Electrochemical characterization

Ink preparation

The catalyst ink for electrode modification was produced through a 20-minute sonication process of 5 mg of catalyst material, 5 μL of Nafion ionomer solution (5 wt%, Sigma-Aldrich), and 495 μL of isopropyl alcohol to achieve a homogeneous ink.

Electrode modification

The Teflon-embedded glassy carbon (GC) disk underwent polishing using 0.3 μm alumina slurry (Buehler) prior to any modifications. The electrode underwent a cleaning process involving immersion in an ultrasonic bath containing Milli-Q water and isopropyl alcohol for 5 minutes to eliminate residual alumina. Subsequently, the object was subjected to a rinsing process using water and later dried to eliminate any residual moisture. A loading of 0.5 mg cm^{-2} was achieved by dispensing the catalyst suspension onto the GC area in five 2 μL increments, totaling 10 μL. Following that, the electrode was subjected to drying in an oven set at 60 °C for 1-2 minutes, followed by air-drying for a minimum of 10 minutes.

Electrochemical measurements

The electrocatalytic activity of the materials was assessed using a standard three-electrode, five-neck cell system that was linked to the Autolab PGSTAT128N potentiostat/galvanostat (Metrohm Autolab B.V., The Netherlands) and managed by Nova 2.1.4 software. In this study, the working electrode was a glassy carbon rotating disk electrode, specifically the OrigaTip model, with a diameter of 5 mm. The reference electrode was a silver-silver chloride electrode, while a GC rod was utilized as the counter electrode. The alkaline electrolyte solution was formulated by dissolving 2.8 g of KOH (with a purity of at least 99.998%, obtained from Sigma-Aldrich) in 500 mL of Milli-Q water. Subsequently, the electrolyte was saturated with either pure oxygen (99.999%, Linde Gas) or deaerated using argon gas (99.999%, Linde Gas).

The ORR polarization curves were recorded in O_2-saturated 0.1 M KOH electrolyte conditions, with a scan rate of 10 mV s^{-1} and at different rotation speeds (360, 610, 960, 1600, 1900, 3100 rpm). Subsequently, an examination was conducted on the OER activity within an Ar-saturated electrolyte containing 0.1 M KOH, utilizing a scan rate of 10 mV s^{-1}. Electrochemical data, where necessary, underwent an 85% iR compensation. The conversion of potentials to RHE was carried out using the following formula:

$E_{Ag/AgCl} = E_{RHE} - 0.966$ ($E_{vsRHE} = E_{vs.Ag/AgCl} + 0.0591*pH + E_{Ag/AgCl}^{\theta}$ (0.209))

The polarization curves were utilized to derive the primary kinetic parameters of the ORR. The parameters under consideration consisted of E_{onset} and $E_{1/2}$, which denote the onset and half-wave potentials, respectively. The overall oxygen electrode bifunctional activity was calculated as the potential difference (ΔE) between the ORR half-wave potential and an OER current density of 10 mA cm^{-2} ($E_{j=10}$): $\Delta E = E_{j=10} - E_{1/2}$.

Assembly of Zn-air battery

The experimental evaluation of the in-house zinc-air battery (ZAB) was conducted using a single-cell battery setup employing a two-electrode configuration. The air cathode, which had a geometric area measuring 3.5 cm^2, was constructed using a nickel mesh current collector and a carbon paper gas diffusion layer known (Sigracet BB39). The cathode layer was coated with an IroNi-3D catalyst ink, with a loading of 2.0 mg cm^{-2}, using the drop-casting method. Subsequently, a hand brush coating technique was employed to ensure the uniformity of the layer. A 99% pure Zn foil was employed as the anode, while a solution of 7 M KOH saturated with ZnO served as the

electrolyte. Zinc oxide (ZnO) was employed to mitigate electrode passivation. The catalyst ink used for the ZAB was prepared by subjecting 7 mg of IrNi-3D electrocatalyst powder to sonication, along with 20 µl of a 5% Nafion ionomer solution (Sigma-Aldrich), 0.2 mL of MilliQ water, and 0.6 mL of ethanol, for 1.5 hours. The benchmark PtRu catalyst ink was prepared using the same procedure with commercial HiSPEC™ 12100, 50% Pt and 25% Ru on a high surface area advanced carbon support, Alfa Aesar.

The battery cell was assembled using a series of stacked plates arranged in the following sequence: a lower plate housing the anode, a middle plate accommodating the electrolyte, a filling neck, an upper plate containing the cathode, and a top plate featuring a 1.8 cm air duct to facilitate airflow. To prevent electrolyte leakage, it is generally imperative to maintain an airtight barrier between the anode and cathode. The galvanostatic tests were conducted under the control of a potentiostat device (PGSTAT128N).

Figures

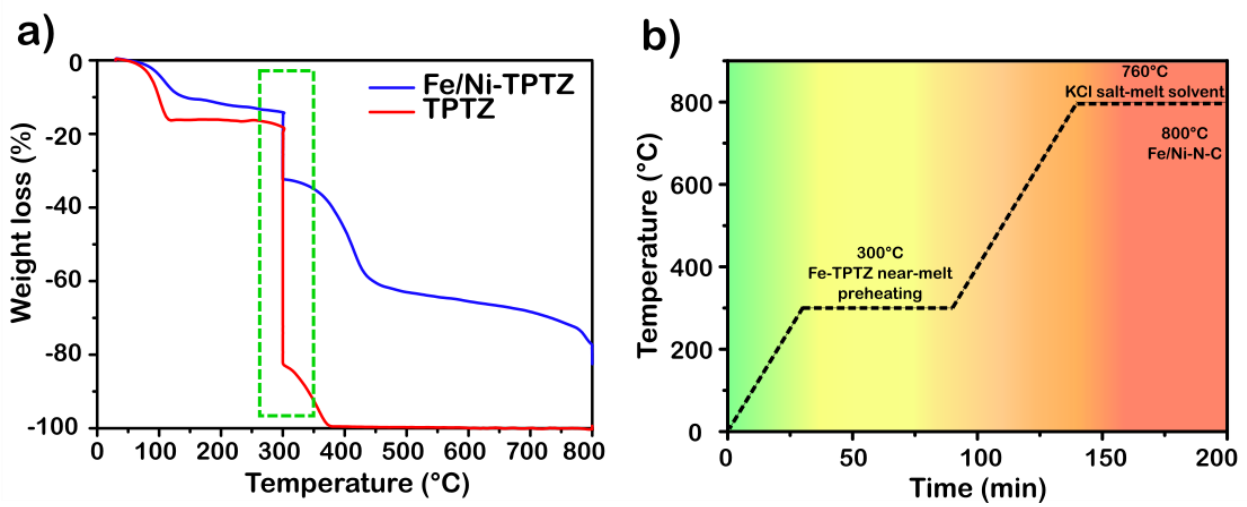

Figure S1. (a) TGA curves of TPTZ and FeNiTPTZ, (b) Pyrolysis protocol for FeNi-N-C synthesis.

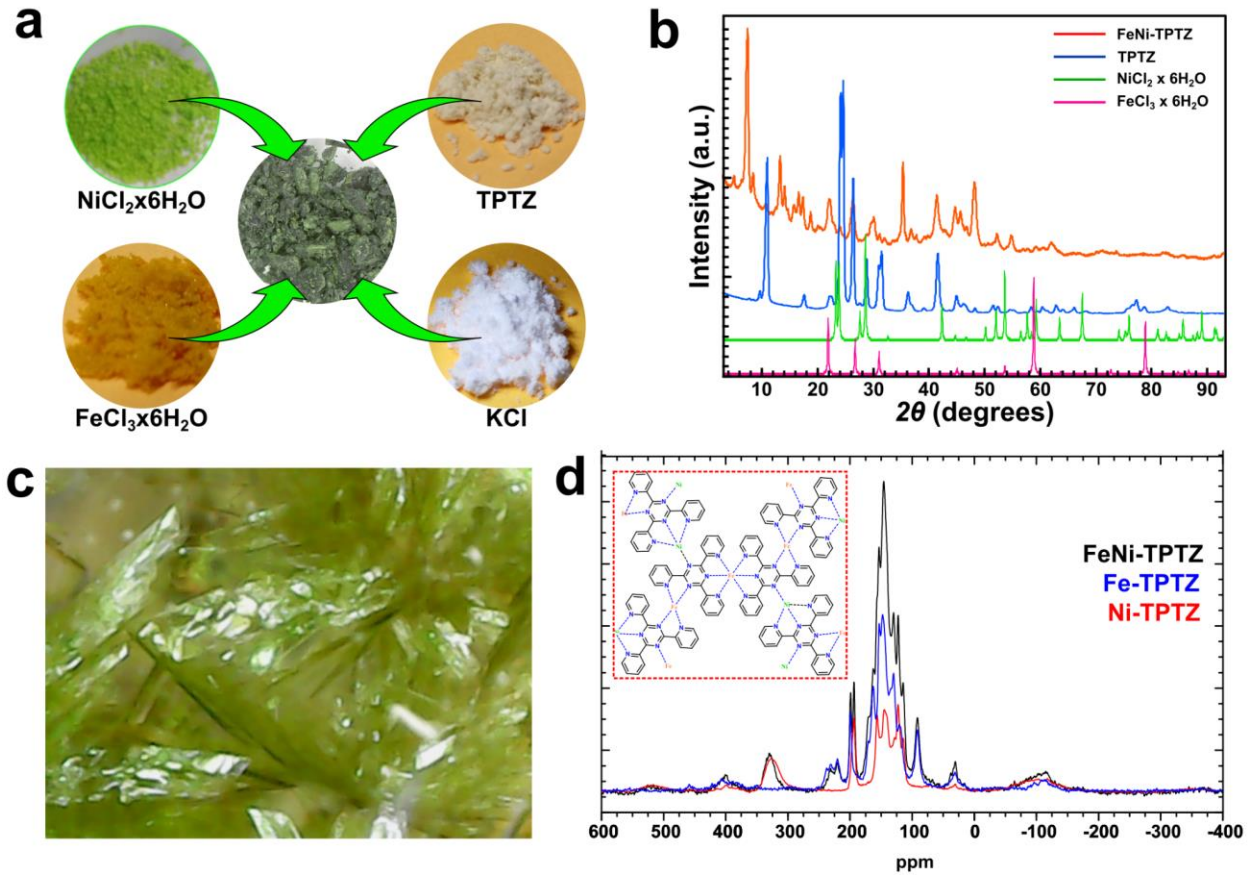

Figure S2. (a) Formation of the colored FeNi-TPTZ complex upon mechanochemical treatment of precursors. (b) Comparative PXRD spectra of reaction precursors and product. (c) Crystals of FeNi-TPTZ. (d) Solid-state NMR of Fe-TPTZ, Ni-TPTZ, and FeNi-TPTZ complex, and suggested structure (inset).

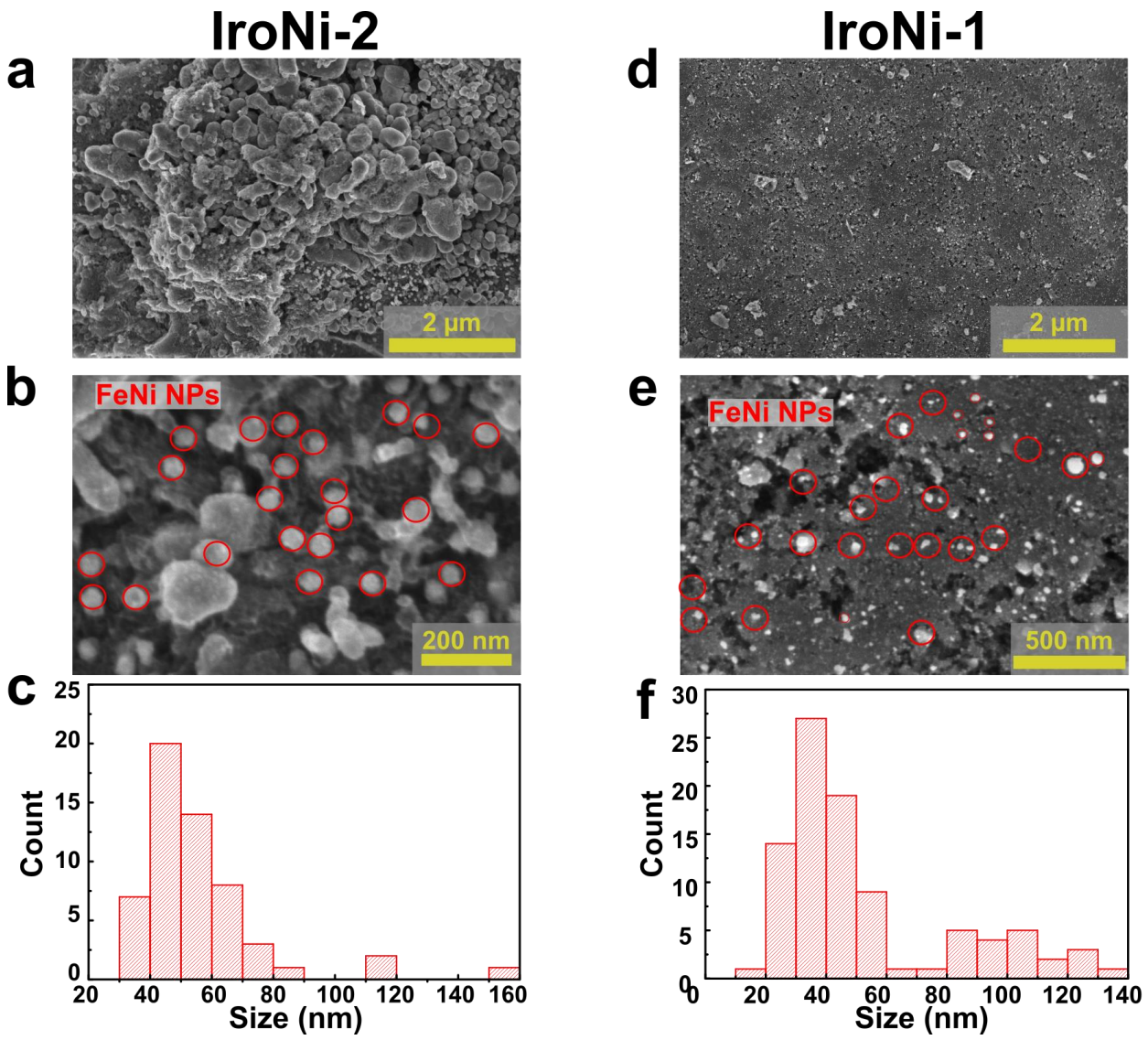

Figure S3. (a,b) SEM images of IroNi-2. (c) FeNi nanoparticle size distribution in IroNi-2 (d,e) SEM images of IroNi-1. (f) FeNi nanoparticle size distribution in IroNi-1.

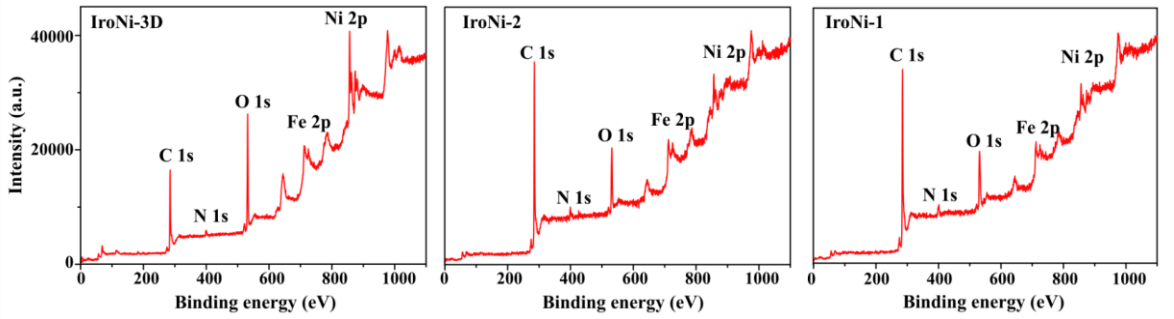

Figure S4. Survey XPS spectra of IroNi samples

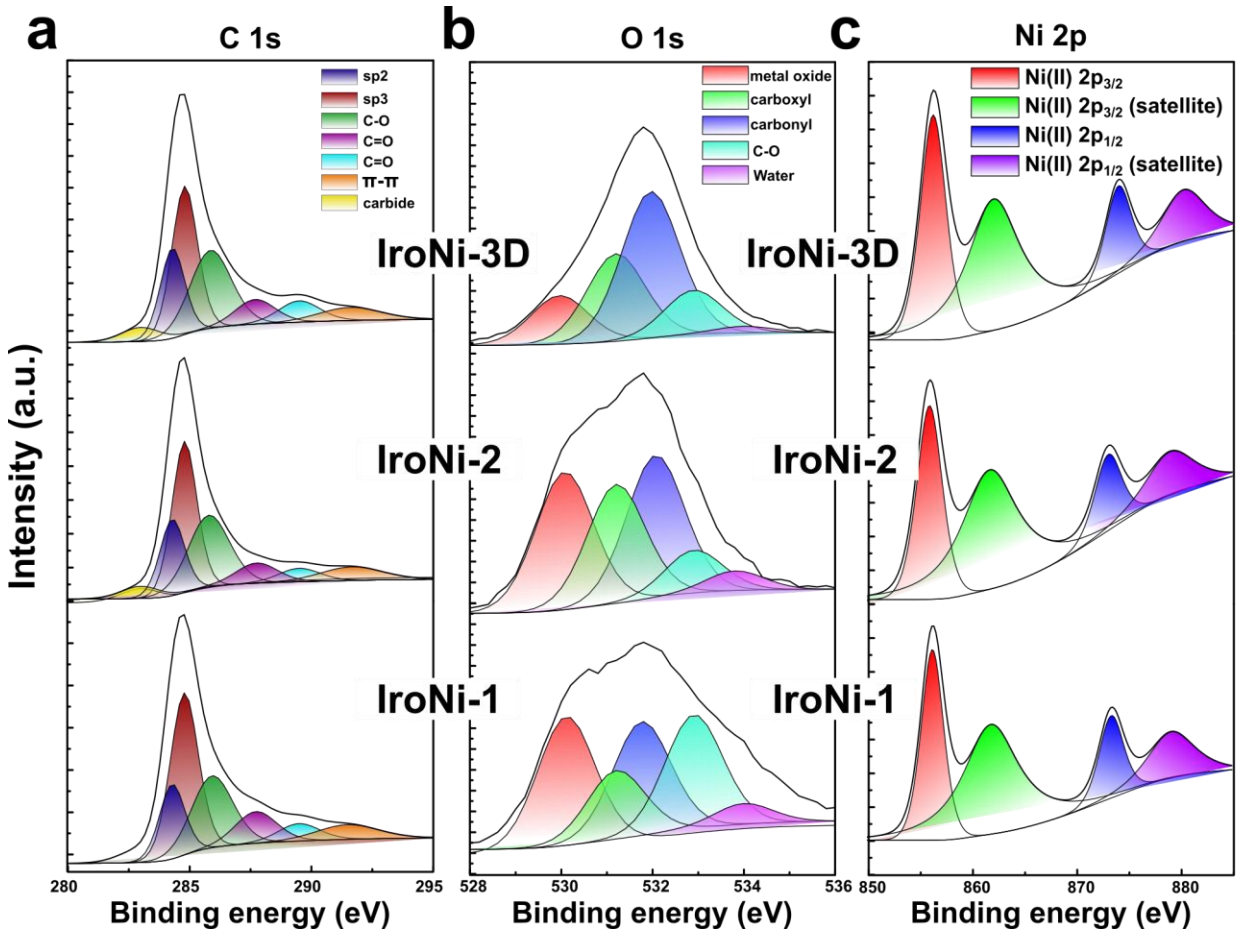

Figure S5. Deconvoluted high-resolution C 1s (a), O 1s (b), and Ni 2p (c) photoelectron spectra of FeNi-N-C catalysts.

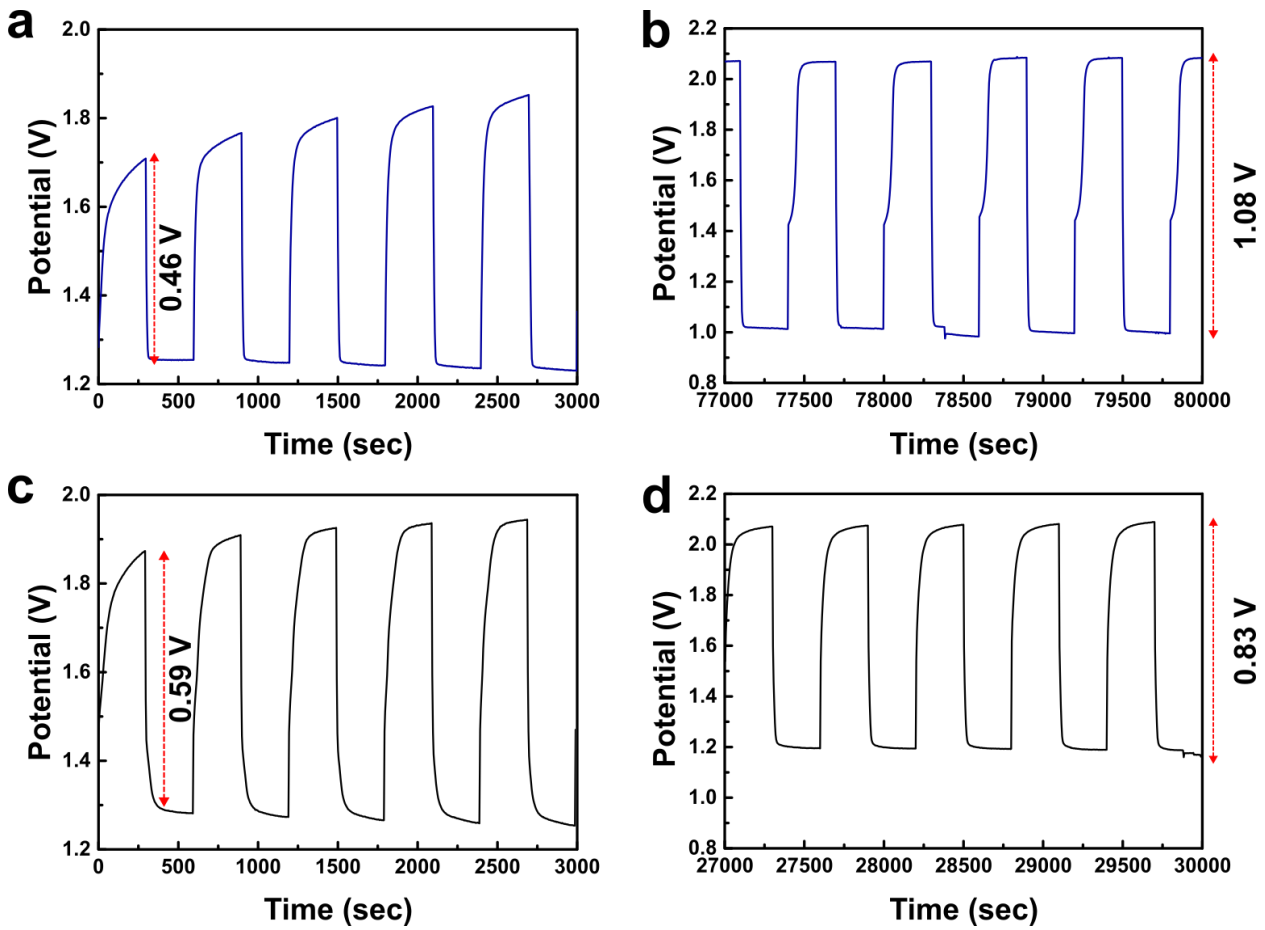

Figure S6. (a) The first cycle, and (b) the final cycle of IroNi-3D ZAB with noted voltage gap difference values at the beginning and the end of the corresponding cycle. (c) The first cycle, and (d) the final cycle of PtRu/C ZAB with noted voltage gap difference values at the beginning and the end of the corresponding cycle.

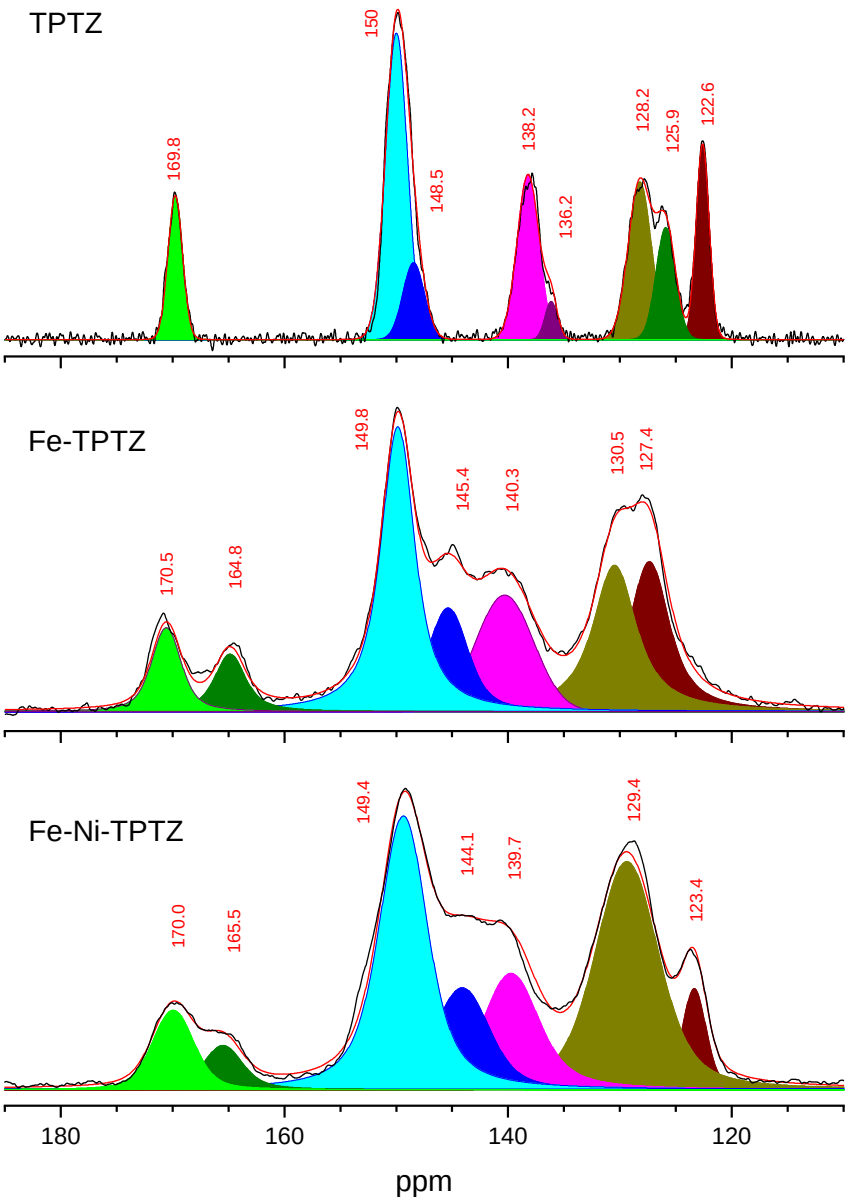

Figure S7. 13C CP-MAS NMR spectra of TPTZ, Fe-TPTZ and Fe-Ni-TPTZ compounds. The spectra show only the resonances of aromatic carbons, which are dipolar coupled with protons.

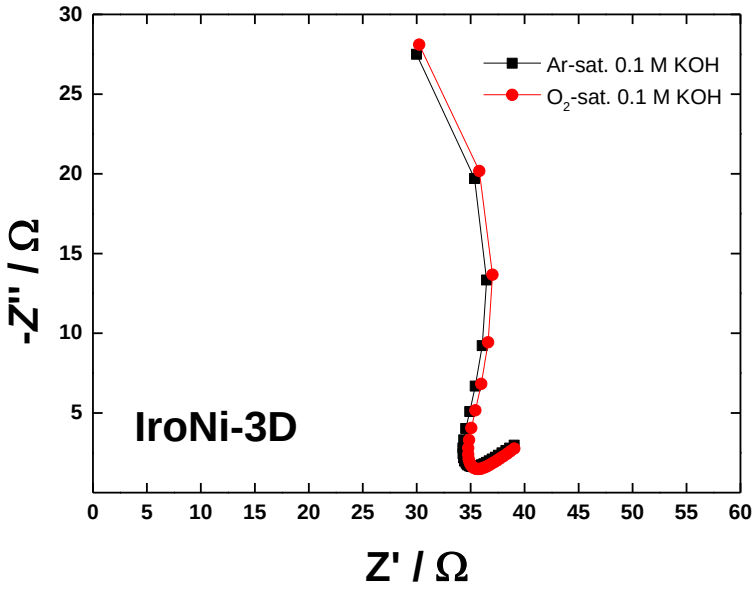

Figure S8. Nyquist plots for IroNi-3D-modified glassy carbon electrode under Ar/O_2.

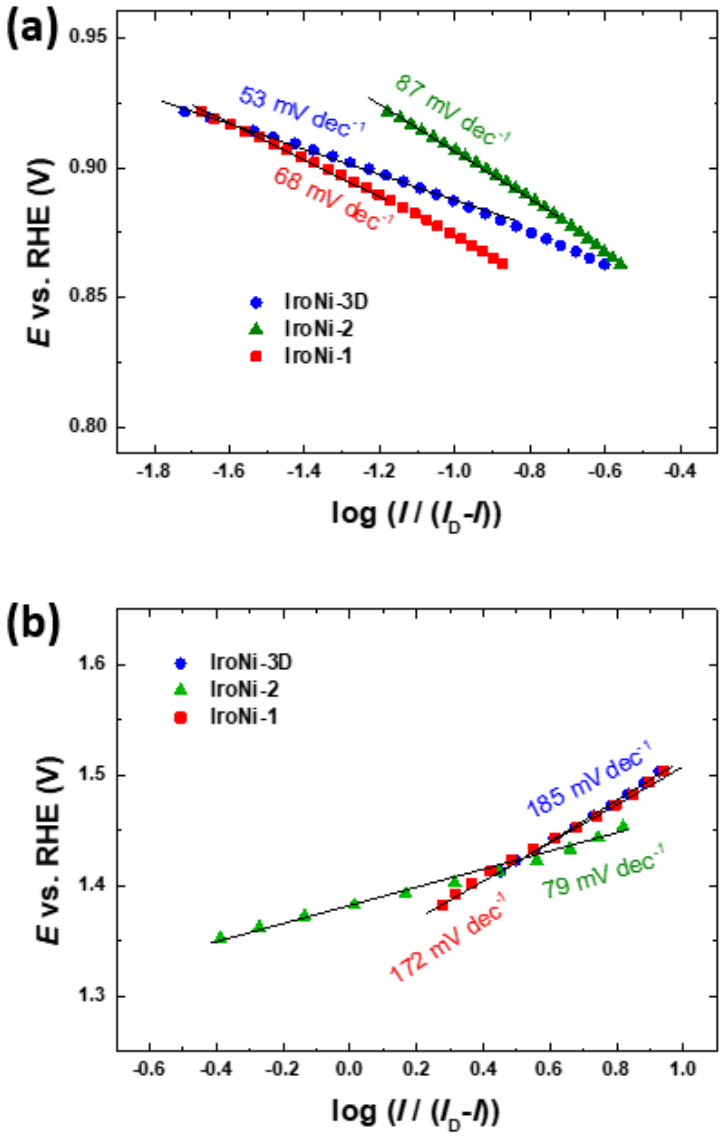

Figure S9. (a) ORR and (b) OER Tafel plots constructed for IroNi catalysts.

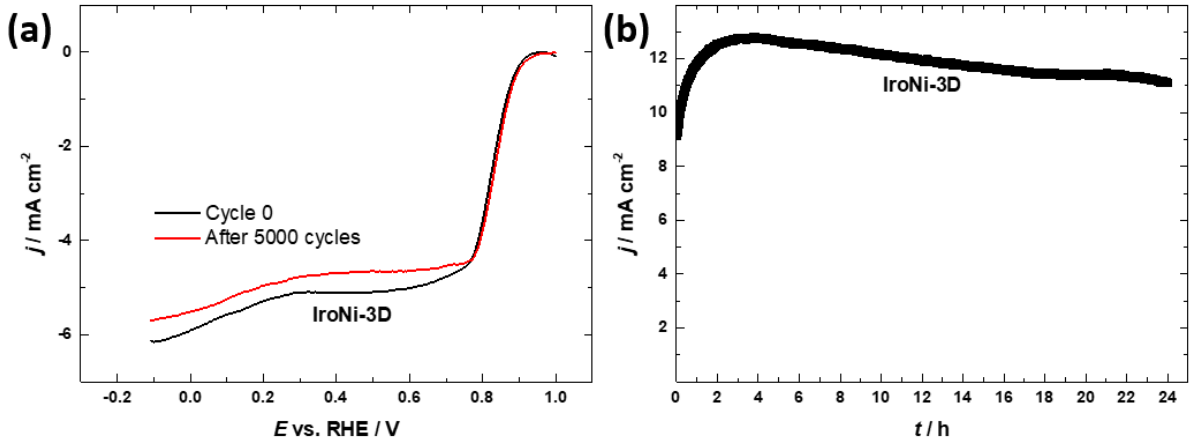

Figure S10. (a) ORR polarization curves obtained for IroNi-3D modified GC electrodes before and after 5000 cycles from 0.6 to 1.0 V vs. RHE (50 mV s^{-1}) in the O_2-saturated 0.1 M KOH solution (ω=1600 rpm); (b) Chronoamperometry curve obtained for IroNi-3D modified electrode at 1.6 V vs. RHE.

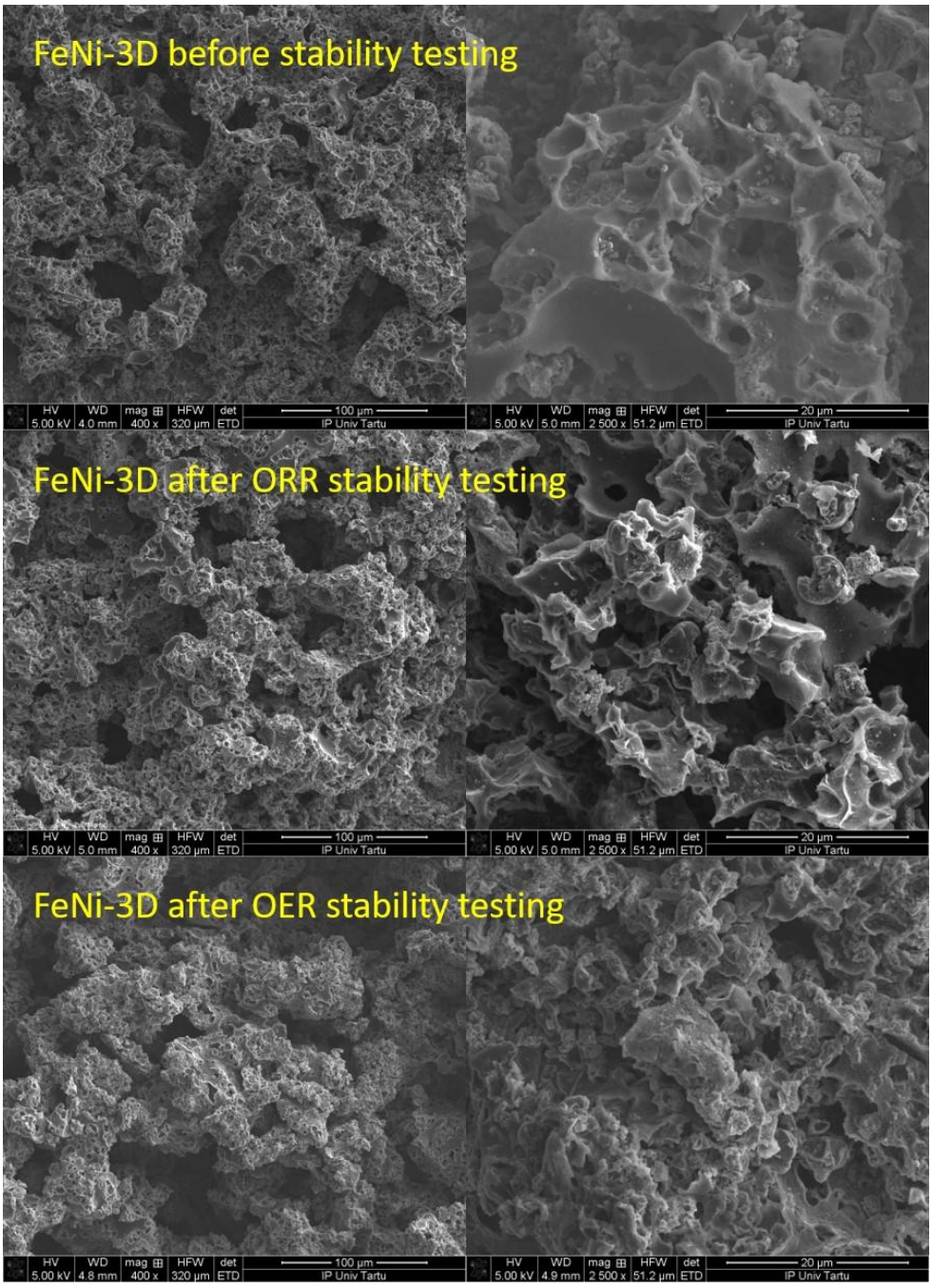

Figure S11. Comparison of surface morphology of IroNi-3D sample before and after stability testing.

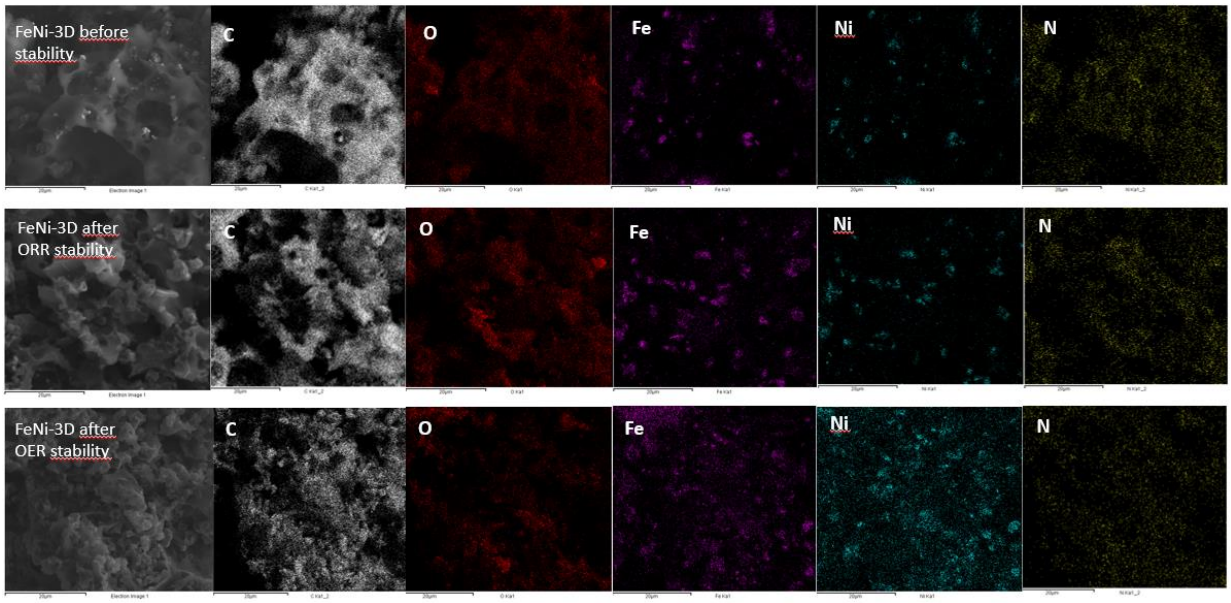

Figure S12. SEM EDX mapping of IroNi-3D sample surface before and after long-term stability tests.

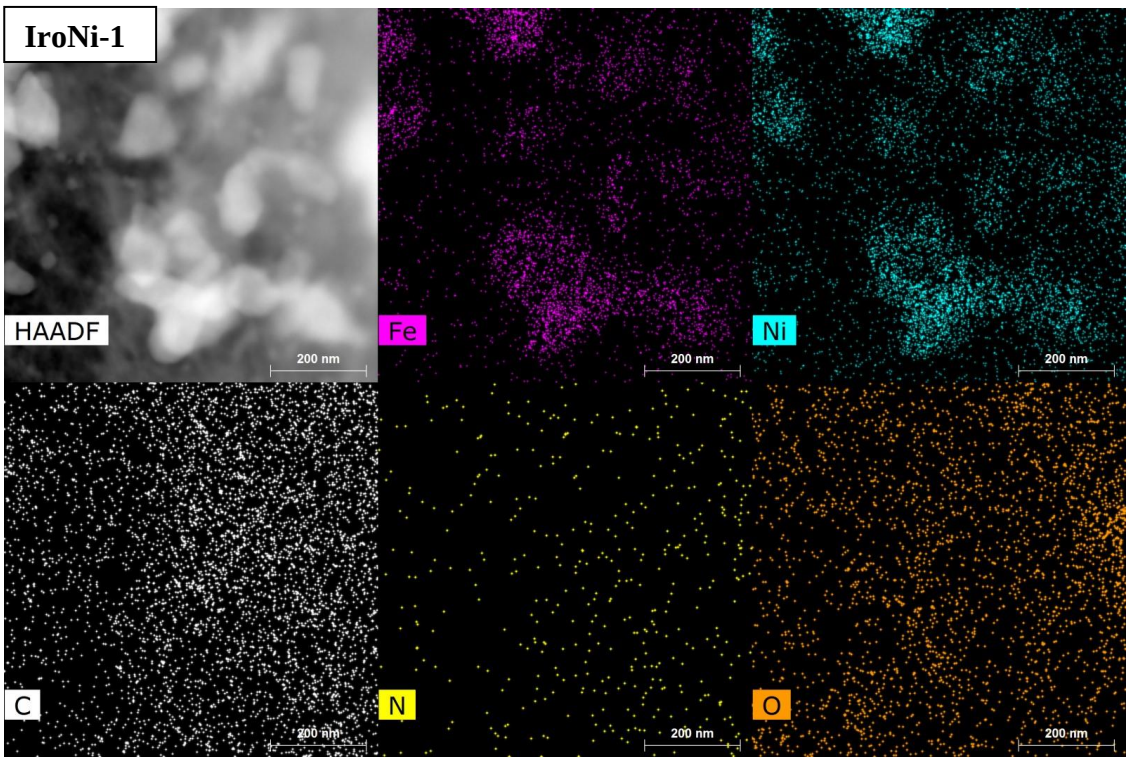

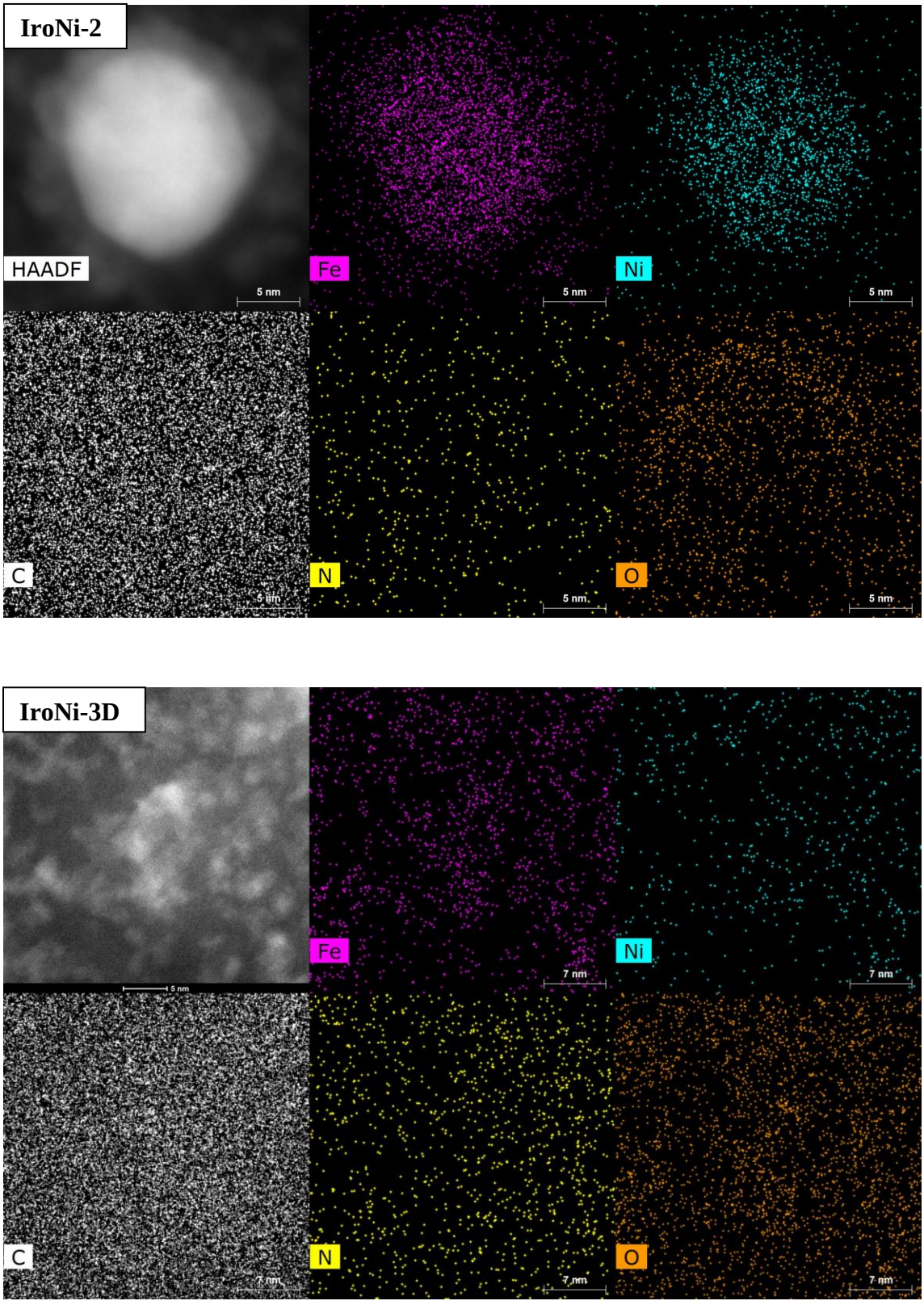

Figure S13. HAADF-STEM images of IroNi-1, IroNi-2 and IroNi-3D catalysts, accompanied by EDS elemental mapping.

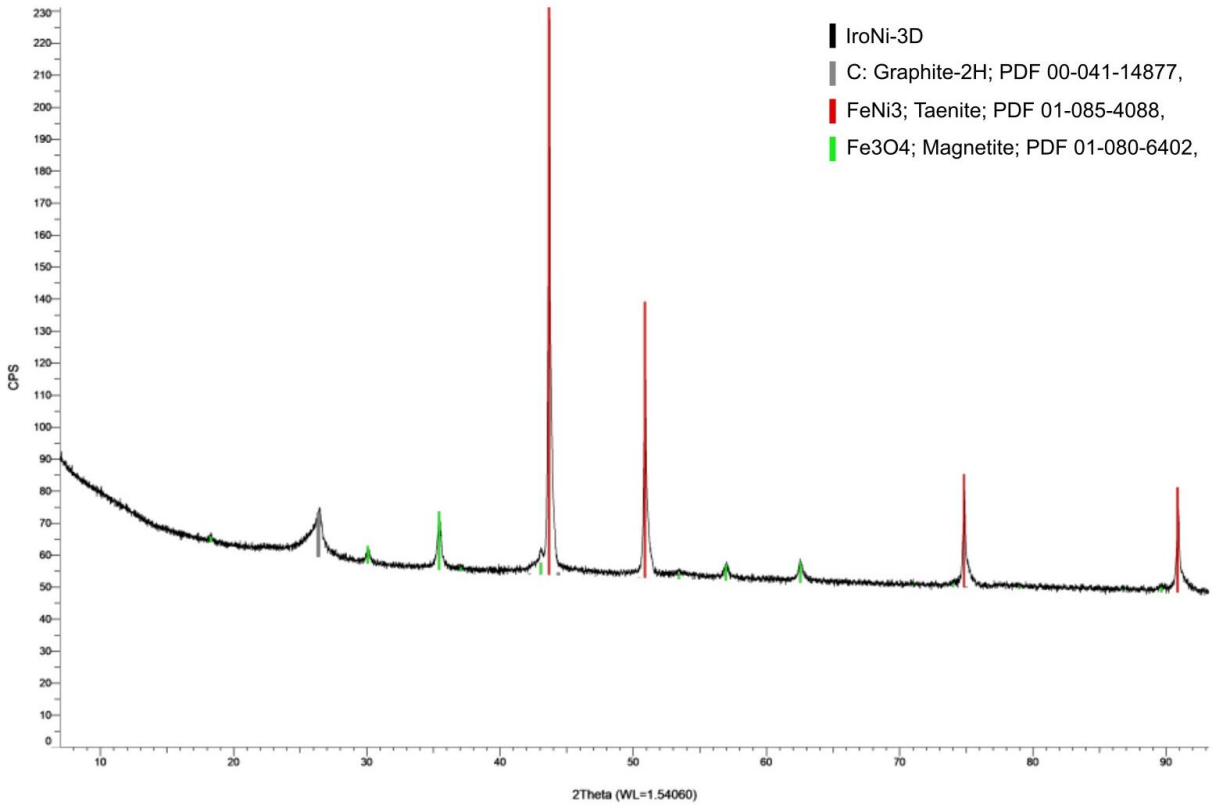

Figure S14. PXRD pattern of IroNi-3D sample, presented alongside reference peaks from the ICDD database (PDF card 01-085-4088; Taenite).

Tables

Table S1. Specific surface area, total pore volume, and average pore size of the catalyst materials were determined from N2 physisorption analysis.

Sample	BET surface area (S_{BET} / m^2 g^{-1})	Total pore volume (cm^3 g^{-1})	$S_{A\ micropores}/S_{A\ mesopores}$ (m^2 g^{-1})
IroNi-3D	570	0.54	148/113
IroNi-2	208	0.35	29/156
IroNi-1	284	0.29	288/194

Table S2. Bulk metal composition of metals (wt%) determined from MP-AES analysis, and surface elemental composition (at%) determined from XPS.

Catalyst	Bulk metal composition of Fe (wt%)	Bulk metal composition of Ni (wt%)	Surface elemental composition (at%)				
			C	N	O	Fe	Ni
IroNi-3D	21.345	20.686	52.6	2.4	28.4	2.3	14.3
IroNi-2	21.636	29.788	77.6	3.0	13.2	2.1	4.1
IroNi-1	29.230	21.065	78.0	3.0	14.3	1.3	3.4

Table S3. Summary of electrochemical performance characteristics of the catalyst samples.

Sample	$E_{1/2}$ (V)	E_{on} (V)	*n*	*ORR Tafel slope (mV dec^{-1})*	$E_{j=10}$ (V)	η_{OER} (V)	ΔE (V)	*OER Tafel slope (mV dec^{-1})*
IroNi-3D	0.82	0.92	3.42	53	1.52	0.29	0.7	185
IroNi-2	0.77	0.93	3.66	87	1.48	0.25	0.71	79
IroNi-1	0.73	0.89	3.72	68	1.51	0.28	0.78	172

Table S4. Summary of electrochemical parameters of the recently published articles reporting on FeNi-N-C type catalyst material.

Sample	$E_{1/2}$ (V vs. RHE)	E_{on} (V vs. RHE)	n	$E_{j=10}$ (V vs. RHE)	η_{OER} (V)	ΔE (V)
IroNi-3D (this work)	**0.82**	**0.92**	**4**	**1.52**	**0.29**	**0.7**
NiO_x@FePc-PI/KB [2]	0.926	-	4	1.515	0.285	0.59
Fe/Ni@NPC-SiO_2/Zn [3]	0.874	-	3.91	1.582	0.352	0.71
ZGNiFe@NG [4]	0.81	-	4	1.65	0.42	0.84
FeNi@NCSs [5]	0.84	0.93	3.91	1.548	0.318	0.708
$NiFe_3$@NGHS-NCNTs [6]	0.823	0.97	3.85	1.613	0.383	0.791
Ni0.6Fe0.4 CM [7]	0.75	0.88	4	1.51	0.28	0.76
Fe,Ni-SAs/DNSC [8]	0.93	1.03	4	1.58	0.350	0.65
NiFe@NCNTs [9]	0.79	-	4.03	1.56	0.330	0.77
Ni-N_4/GHSs/Fe-N_4 Janus [10]	0.83	0.93	3.70	1.62	0.39	0.79

Ni_3Fe-GA_1 [11]	0.8	0.93	3.5	1.469	0.239	0.74
$FeNi_3N$/NG [12]	0.79	0.88	3.73	1.64	0.410	0.85
FeNi-NC [13]	0.83	0.98	3.97	1.61	0.380	0.81
FeNi/N−C [14]	0.81	0.90	3.9	1.643	0.413	0.87

Table S5. Summary of catalyst performance in ZAB and comparison with previously reported materials.

Catalyst	**Zinc-air battery**	
	Electrolyte	**Power Density (mW cm^{-2})**
IroNi-3D (this work)	**7 M KOH + ZnO (sat.)**	**144.0**
NiO_x@FePc-PI/KB [2]	6 M KOH + 0.2M $Zn(OAc)_2$	232.9
Fe/Ni@NPC-SiO_2/Zn [3]	18 M KOH + 0.02 M $Zn(OAc)_2$	83.5
ZGNiFe@NG [4]	P-(AM-co-AA)/6 M KOH	84.95
FeNi@NCSs [5]	6 M KOH + 0.2 M $Zn(OAc)_2$	128.8
$NiFe_3$@NGHS-NCNTs [6]	6 M KOH + 0.2 M $Zn(OAc)_2$	126.54
Ni0.6Fe0.4 CM [7]	6 M KOH + 0.2 mol $Zn(OAc)_2$	59.83
Fe,Ni-SAs/DNSC [8]	6 M KOH	160
NiFe@NCNTs [9]	6 M KOH	360.12
Ni_3Fe-GA_1 [11]	6 M KOH + 0.2M $Zn(OAc)_2$	62.9
$FeNi_3N$/NG [12]	6 M KOH + 0.2M $Zn(OAc)_2$	115.3
FeNi-NC [13]	6 M KOH with 0.2 M ZnO	80.8

FeNi/N−C [14]	6 M KOH with 0.2 M ZnO	109.6

References

[1] A.V. Neimark, Y. Lin, P.I. Ravikovitch, M. Thommes, Quenched solid density functional theory and pore size analysis of micro-mesoporous carbons, Carbon. 47 (2009) 1617–1628. https://doi.org/10.1016/j.carbon.2009.01.050.

[2] Z. Zhang, T. Wang, W. Wang, X. Wang, X. Luo, C. Cheng, X. Liu, A Stable Imide-Linked Metalphthalocyanine Framework with Atomically Dispersed Fe-N4 Sites and Ultrafine Nickel Oxide Nanoparticles to Boost Reversible Oxygen Electrocatalysis with a Record-Low ΔE of 0.59 V, Advanced Energy Materials. 13 (2023) 2300325. https://doi.org/10.1002/aenm.202300325.

[3] B. Guo, J. Guo, W. Yang, X. Tian, X. Wang, Z. Xiang, M. Wu, Highly dispersed iron/nickel dual-sites in hierarchical porous carbon materials as high-performance bifunctional oxygen electrocatalysts for Zn-air batteries, Renewable Energy. 201 (2022) 117–124. https://doi.org/10.1016/j.renene.2022.11.036.

[4] W. Li, Y. Wu, M. Chen, P. Dai, T. Jiang, S. Zhou, Ultrathin nitrogen-doped defective carbon layer embedded with NiFe for solid zinc-air batteries, Journal of Alloys and Compounds. 925 (2022) 166658. https://doi.org/10.1016/j.jallcom.2022.166658.

[5] S.-Y. Lin, X. Zhang, S.-Y. Sang, L. Zhang, J.-J. Feng, A.-J. Wang, Bio-derived FeNi alloy confined in N-doped carbon nanosheets as efficient air electrodes for Zn–air battery, Journal of Colloid and Interface Science. 628 (2022) 499–507. https://doi.org/10.1016/j.jcis.2022.07.180.

[6] Y. Ma, W. Chen, Z. Jiang, X. Tian, X. WangGuo, G. Chen, Z.-J. Jiang, NiFe nanoparticles supported on N-doped graphene hollow spheres entangled with self-grown N-doped carbon nanotubes for liquid electrolyte/flexible all-solid-state rechargeable zinc–air batteries, J. Mater. Chem. A. 10 (2022) 12616–12631. https://doi.org/10.1039/D2TA03110H.

[7] Y. Li, Q. Zou, Z. Li, D. Xie, Y. Niu, J. Zou, X. Zeng, J. Huang, MOF derived Ni-Fe based alloy carbon materials for efficient bifunctional electrocatalysts applied in Zn-air battery, Applied Surface Science. 572 (2022) 151286. https://doi.org/10.1016/j.apsusc.2021.151286.

[8] X. Zhang, Y. Li, M. Jiang, J. Wei, X. Ding, C. Zhu, H. He, H. Lai, J. Shi, Engineering the coordination environment in atomic Fe/Ni dual-sites for efficient oxygen electrocatalysis in Zn-air and Mg-air batteries, Chemical Engineering Journal. 426 (2021) 130758. https://doi.org/10.1016/j.cej.2021.130758.

[9] M. Jiang, Z. Tan, M. Cao, A robust bifunctional electrocatalyst for rechargeable zinc-air batteries: NiFe nanoparticles encapsulated in nitrogen-doped carbon nanotubes, International Journal of Hydrogen Energy. 46 (2021) 15507–15516. https://doi.org/10.1016/j.ijhydene.2021.02.079.

[10] J. Chen, H. Li, C. Fan, Q. Meng, Y. Tang, X. Qiu, G. Fu, T. Ma, Dual Single-Atomic Ni-N4 and Fe-N4 Sites Constructing Janus Hollow Graphene for Selective Oxygen Electrocatalysis, Advanced Materials. 32 (2020) 2003134. https://doi.org/10.1002/adma.202003134.

[11] Z. Wang, X. Liao, Z. Lin, F. Huang, Y. Jiang, K.A. Owusu, L. Xu, Z. Liu, J. Li, Y. Zhao, Y.-B. Cheng, L. Mai, 3D Nitrogen-Doped Graphene Encapsulated Metallic Nickel–Iron Alloy Nanoparticles for Efficient Bifunctional Oxygen Electrocatalysis, Chemistry – A European Journal. 26 (2020) 4044–4051. https://doi.org/10.1002/chem.201904722.

[12] L. Liu, F. Yan, K. Li, C. Zhu, Y. Xie, X. Zhang, Y. Chen, Ultrasmall FeNi3N particles with an exposed active (110) surface anchored on nitrogen-doped graphene for multifunctional electrocatalysts, J. Mater. Chem. A. 7 (2019) 1083–1091.

https://doi.org/10.1039/C8TA10083G.
[13] L. Yang, X. Zeng, D. Wang, D. Cao, Biomass-derived FeNi alloy and nitrogen-codoped porous carbons as highly efficient oxygen reduction and evolution bifunctional electrocatalysts for rechargeable Zn-air battery, Energy Storage Materials. 12 (2018) 277–283. https://doi.org/10.1016/j.ensm.2018.02.011.
[14] C. Zhang, C. Wu, Y. Gao, Y. Gong, H. Liu, J. He, FeNi Nanoparticles Coated on N-doped Ultrathin Graphene-like Nanosheets as Stable Bifunctional Catalyst for Zn-Air Batteries, Chemistry – An Asian Journal. 16 (2021) 1592–1602. https://doi.org/10.1002/asia.202100347.